doi.org/10.36721/PJPS.2023.36.6.SP.1875-1883.1

Moringa oleifera-mediated iron oxide nanoparticles, characterization and their anti-proliferative potential on MDA-MB 231 human breast cancer cells

Huzaifa Umar[1]* and Maryam Rabiu Aliyu[2]
[1]Operational Research Center in Healthcare, Near East University, TRNC Mersin 10, Nicosia, Turkey
[2]Department of Energy System Engineering Cyprus International University, Nicosia, Northern Cyprus via Mersin 10, Turkey

Abstract: Iron oxide nanoparticles (Fe_2O_3 NPs) stabilized with *Moringa oleifera* (M.O.) were successfully synthesized. The study aimed to explore the cytotoxic, anti-proliferative and anti-microbial potential of Fe_2O_3 NPs through various assays, including trypan blue, 3-[4,5-dimethylthiazol-2-yl]-2,5-diphenyltetrazolium bromide (MTT), wound healing and disc diffusion assay. The *Moringa oleifera*-mediated Fe_2O_3 NPs (M O Fe2O3 NPs) underwent analysis using various techniques, including Fourier-transform infrared spectroscopy (FTIR), X-ray diffraction (XRD), UV-vis spectroscopy (UV-vis), scanning electron microscopy (SEM) and energy-dispersive X-ray spectroscopy (EDX). FTIR, XRD and SEM-EDX results confirmed the successful synthesis of Fe_2O_3 NPs. The UV-Vis spectra analysis indicated an absorption peak at 314 nm, ensuring both the successful synthesis and remarkable stability of the nanoparticles. The nanoparticles displayed a uniform spherical morphology and contained Fe, O, confirming the formation of M O Fe_2O_3 NPs. Cytotoxic and anti-proliferative potential on MDA-MB 231 human breast cancer cells were observed with various concentrations of M O Fe_2O_3 NPs and the cytotoxicity result revealed an IC_{50} of 69.7µg/mL. In conclusion, stable Fe_2O_3 NPs were synthesized using a methanolic extract of M.O. and they demonstrated antimicrobial activity against both gram-negative and gram-positive bacteria. The nanoparticles exhibited cytotoxicity and anti-proliferative activity on MDA-MB 231 human breast cancer cell lines.

Keywords: Wound heal, UV-vis spectroscopy, trypan blue, spherical morphology, fourier-transform infrared spectroscopy.

INTRODUCTION

Medical researchers have become increasingly interested in nanomaterials owing to their advantageous properties. These materials, such as nanoparticles (NPs), possess a size similarity to biological molecules like enzymes, proteins and lipids, enabling more effective interactions. Unlike conventional drugs, nanomaterials are characterized by their smaller size, extensive surface area and distinctive magnetic, physicochemical, catalytic and mechanical properties. Moreover, they exhibit enhanced accumulation in targeted organs, contributing to their overall effectiveness (Alphandéry, 2020; Priya *et al*., 2021). Nanoparticles (NPs) have become valuable tools for bridging materials across scales, ranging from large to atomic dimensions. Various precursors, including iron, nickel, zinc, copper, silver and gold nanoparticles, are widely used in their synthesis due to the favorable properties of these precursors and their applicability across a wide range of uses (Devatha *et al.*, 2017). The growing trend of adopting environmentally friendly approaches in nanotechnology has led to the development of non-toxic and stable metal oxide nanoparticles (MO NPs). These particles exhibit unique physical and chemical properties that make them compatible with the human body, opening up diverse applications in areas such as cancer treatment, drug delivery, medical imaging, diabetes treatment, biosensors, antimicrobial agents and cosmetics (Umar *et al.*, 2019).

Hematite iron oxide, particularly in its α- Fe_2O_3 form, is a thermodynamically stable substance exhibiting n-type semiconductor properties (Gullu and Parlak, 2016). This iron oxide variant possesses a core and shell structure, consisting of hydrous iron oxides and metallic iron (Li and Zhang, 2006). Hematite nanoparticles (Fe Fe_2O_3 NPs) can be effectively synthesized through controlled precipitation methods involving inorganic metal salts or material washing and their size can be adjusted through calcination. It is crucial to note that the choice of the synthetic method significantly influences the quality of the nanoparticles. Therefore, improving the synthetic approach can lead to a substantial enhancement in nanoparticle quality (Morales Morales, 2017). Due to their biocompatibility, the therapeutic properties of iron oxide nanoparticles have been extensively explored, making them highly favored for treating various medical conditions (Alphandéry, 2020). In cancer treatment, Fe2O3 NPs have been investigated for their ability to generate reactive oxygen species or localized heat. Combining Fe_2O_3 NPs with chemotherapeutic drugs, such as paclitaxel (Fe_2O_3 NPs-PAX), has shown enhanced effectiveness in vitro on human prostate cancer cells (PC3

**Corresponding author:* e-mail: huzaifa.umar@neu.edu.tr

and CWR22R) and in vivo on xenograft tumors in mice derived from C4-2 cells. Similarly, the combination of Fe2O3 NPs with cisplatin demonstrated increased cytotoxicity toward A549 cells compared to free cisplatin (Chowdhury *et al*., 2017; El-Zahaby *et al.,* 2019). Conventional methods of producing metal oxide nanoparticles involve costly and hazardous physical and chemical techniques, often utilizing antagonistic chemicals as stabilizers (Suresh *et al*., 2018).

The integration of biosynthesis, green chemistry, nanoscience and technology has established a comprehensive network of interconnected fields aimed at mitigating the hazardous effects associated with chemically synthesized nanoparticles. This eco-friendly approach is not only cost-effective and safe but also stands out as a preferred method over alternative techniques (Kumar *et al*., 2022). The progress in biomedical research represented by the development of metallic oxide nanomaterials, such as Fe_2O_3 NPs, through green routes is noteworthy (Zangeneh *et al.*, 2020). In the biomedical field, iron oxide holds crucial significance for applications in diagnostics, treatments, drug delivery and bioremediation (Zangeneh *et al.*, 2020). The synthesis of nanoparticles raises substantial concerns, with biological methods being recognized as eco-friendly in contrast to the perceived toxicity of chemical approaches (Dowlath *et al*., 2021). Plants are increasingly acknowledged as convenient and accessible resources for nanoparticle production, offering ease of handling, minimal risks and cost-effectiveness, making them an attractive option for many (Kharey *et al*., 2022). The bioactive compounds present in plant extracts provide numerous health benefits and serve dual roles as capping and reducing agents during synthesis. This dual function helps prevent agglomeration and imparts crucial stability to the resulting nanoparticles (Conde-Cid *et al*., 2021).

Moringa oleifera (M.O.) is a swiftly growing softwood plant predominantly found in tropical and subtropical regions. In recent years, this plant has garnered increasing attention from researchers in the field of animal husbandry due to its comprehensive nutritional, antioxidative and medicinal attributes (Makkar and Becker, 1997). Despite its widespread applications in food and medicines, there is a scarcity of clinical trials studying the effectiveness of M.O. leaf and other products in treating malnutrition and showcasing their undeniable therapeutic potential in humans. The seed oil of M.O., rich in oleic acid at 72%, is extensively utilized for medicinal purposes in African and Asian countries due to its significant medicinal importance (Karima *et al*., 2021). Various parts of M.O. have been utilized as a rich source of distinct glucosinolates, flavonoids, phenolic acids, polyunsaturated fatty acids (PUFAs), tocopherols, essential minerals and folate (Amaglo *et al*., 2010; Coppin *et al*., 2013, Saini *et al*., 2016). The leaves aqueous extract, in particular, was found to contain 1.66% isothiocyanates and 3.82% total polyphenols (Waterman *et al*., 2014). Glucosinolates, specifically glucomoringin and isothiocyanates are prevalent in various parts such as foliage, flowers, fruits, seeds and bark of M.O. (Amaglo *et al*., 2010). While benzyl glucosinolate (glucotropaeolin) is notably present in the roots, the highest concentration of glucosinolate is reported in the leaves and seeds. The enzymatic catabolism of glucosinolates by myrosinase results in the production of isothiocyanates, nitriles and thiocarbamates (Dhakad *et al*. 2019). Traditionally, M.O. leaves have been employed for the treatment of various ailments, including nervous debility, paralysis, asthma, diabetes, blood pressure issues, diarrhoea, fever, cough, cholera, spasms, enlarged liver and spleen, infections and ulcers, inflammation and to facilitate wound healing (Mishra *et al*., 2011; Promkum *et al*., 2010).

In our current study, Fe_2O_3 nanoparticles (NPs) were synthesized, employing M.O. methanolic extract as a stabilizing agent. Various spectroscopic and microscopic methods were employed to characterize the synthesized *Moringa oleifera*-mediated iron oxide nanoparticle (MO Fe_2O_3 NPs). Our assessment of the MO Fe_2O_3 NPs and the extract revealed their potential to inhibit cell migration and cell proliferation and induce cytotoxic effects on MDA-MB 231 cells. These evaluations were conducted using wound heal, (3-[4,5-dimethylthiazol-2-yl]-2,5-diphenyltetrazolium bromide) MTT and trypan blue assay. Furthermore, we investigated the antimicrobial properties of the MO Fe_2O_3 NPs against *Escherichia coli* and *Bacillus cereus*, employing standard methods.

MATERIALS AND METHODS

Materials

Fresh *Moringa oleifera (*M.O.) leaves were collected from a Bauchi State (0° and 36′N; Long 10° and 00′E) in August, 2021, Nigeria and authenticated by Asst. Prof. Dr. Emmanuel Mishelia of the Pharmaceutical Botany Department Herbarium of Cyprus International University and a voucher number of CIU/PHARM/MORI/001 were given to the specimen and kept at the herbarium of the institute. All the aqueous solutions were prepared using de-ionized water.

All chemicals and reagents used throughout the experiment are of analytical grades. The chemicals used include: Iron (III) chloride ($FeCl_3$) (Merc), Dimethyl Sulfoxide (DMSO) (Sigma-Aldarich Inc.), Dulbecco's Modified Eagle Medium (DMEM) (Gibco by Life Technologie, USA), Fetal Bovine Serum (FBS) (Gibco by Life Technologies, USA), Glycine (Sigma-Aldarich Inc.), 0.25% Trypsin and 0.4 % Tryphan Blue (Gibco by Life Technologies, USA), L-Glutamine 200 mm (Gibco by Life Technologies, USA), Distilled Water (Gibco by Life Technologies, USA), 70% Ethanol (Merck), Penicillin (Gibco by Life Technologies, USA).

Biosynthesis of iron oxide nanoparticles

Fe_2O_3 NP synthesis with M.O. leaves *(*MO Fe_2O_3 NPs) was achieved using the method employed by (Aisida *et al.*, 2019) with some modifications. M.O. leaves collected were weighed, dried, pulverized to powder (fig. 1) and extracted in aqueous medium in an Erlenmeyer flask. Biosynthesis of Fe_2O_3 NPs was carried out using 0.001 M ferric chloride solution and 20% M.O. methanolic extract. After being centrifuged at 10,000 rpm for 30 minutes, the mixture underwent 2-3 washes with Millipore water to eliminate impurities and was kept at 180℃ for five hours.

Fig. 1: *Moringa oleifera* leaves and pulverized powder

Characterization of iron oxide nanoparticles

The UV-Vis spectroscopy analysis of the synthesized Moringa Oleifera-stabilized Fe_2O_3 nanoparticles (MO Fe_2O_3 NPs) was carried out using a Shimadzu UV-2450 instrument. The NPs were dissolved in deionized water and subjected to sonication for thorough mixing. The resulting solution was then filtered and transferred into a 10 mm cuvette, where the spectrum was measured within the wavelength range of 200 to 900 nm at room temperature. Additionally, the functional groups present in the M O Fe_2O_3 NPs were identified using a Fourier Transform Infrared Spectrophotometer (FTIR) operating at a frequency range of 500-4000 cm^{-1}. To evaluate the crystalline nature of the M O Fe_2O_3 NPs, the Rigaku ZSX Primus II X-ray diffractometer (XRD) was employed. Powdered samples were utilized in the X-ray diffractometer, equipped with CuK radiation, to investigate the structural characteristics of the nanoparticles. Furthermore, the morphological structure of the nanoparticles was analyzed using a scanning electron microscope (SEM) and elemental mapping was performed through energy-dispersive X-ray spectroscopy (EDX).

Determination of antimicrobial activity

Antimicrobial activity of MO Fe_2O_3 NPs on *Bacillus cereus* (ATCC 9634) and *Escherichia coli* (O157:H7) was carried out on muller hinton agar as revealed by (Umar *et al.*, 2022). After treating the organisms with Fe_2O_3 NPs and letting them incubate overnight, inhibition zones were evaluated following standard microbiology-based protocols by NCCLS (National Committee for Clinical Laboratory Standards) recommended by WHO.

Cytotoxicity, Proliferation* and *anti-migratory assay

We assessed the effect of synthesized M O Fe_2O_3 NPs on MDA-MB 231 cells by employing a modified procedure based on the method described by Umar *et al*. (2023). These cells were subjected to varying concentrations of the extract, specifically 500, 250, 50 and 10µg/mL and then incubated for 24 hours. Following removing the treatment, we introduced diluted trypan blue and incubated it for 10 minutes in darkness. Subsequently, we count the number of both dead and viable cells.

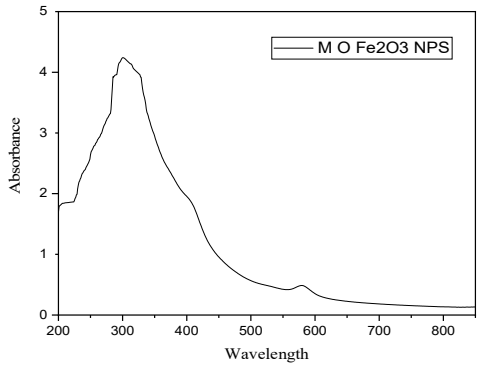

Fig. 2: UV-Vis spectrum of the synthesized MO Fe_2O_3 NPs.

Abbreviation: UV-Vis, UV-vis spectroscopy (UV-vis); M O Fe_2O_3-NPs, *Moringa oleifera* Iron oxide nanoparticles.

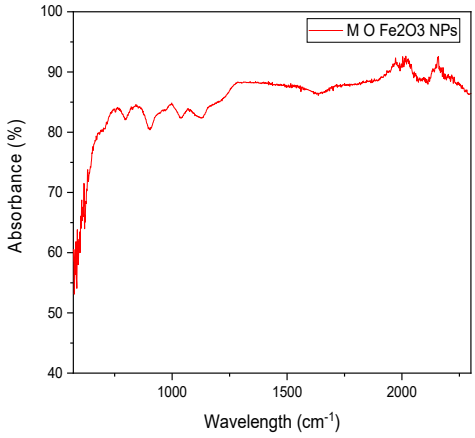

Fig. 3: FT-IR spectra of the synthesized M O Fe_2O_3-NPs.

Abbreviation: FT-IR, Fourier-transform infrared spectroscopy; MO Fe_2O_3-NPs, *Moringa oleifera* Iron oxide nanoparticles.

Cell proliferation after exposure to various Fe_2O_3 NPs concentrations was evaluated in MDA-MB 231 cells using the methodology detailed in Umar *et al*.'s studies with slight modification (Umar *et al*., 2019). Specifically, cells were treated with Fe_2O_3 NPs at 500, 250, 50 and 10 µg/mL concentrations, with an initial cell count of 3 x 10^4. Following removing the culture medium, we introduced 600 µL growth media and 5mg/mL of MTT to the cells. After the incubation period, the MTT solution

was aspirated and a mixture of DMSO (890µL) and glycine buffer (110µL) was added. Additionally, we measured absorbance at 570nm using an Absorbance Micro plate Reader (ELX 800^{TM}). Multiple measurements were conducted.

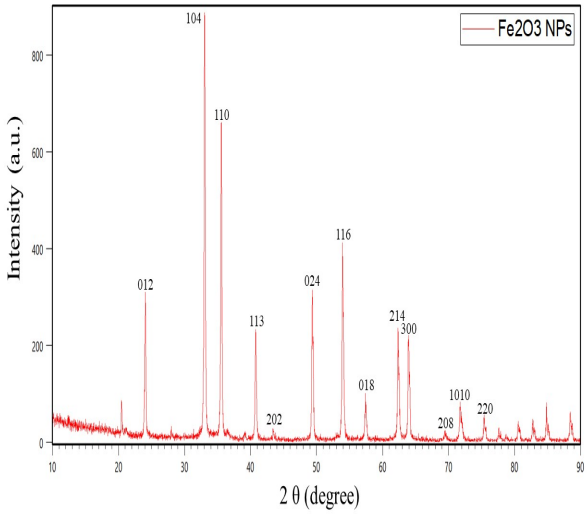

Fig. 4: XRD image of the synthesized Fe_2O_3 NPs.
Abbreviation: XRD, X-ray diffraction; Fe_2O_3-NPs, Iron oxide nanoparticles.

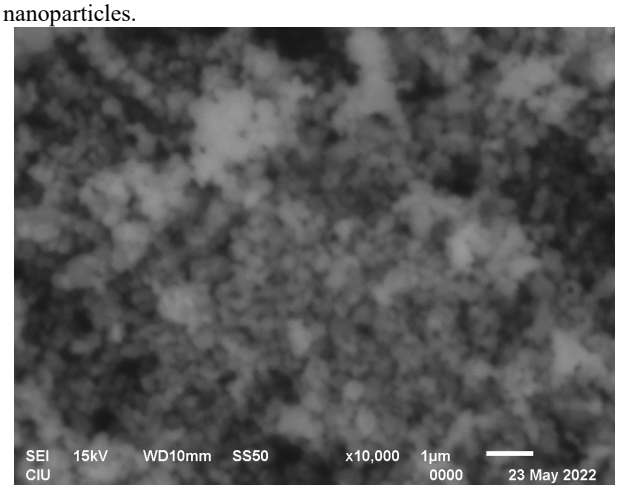

Fig. 5: SEM image of the synthesized M O Fe_2O_3-NPs.
Abbreviation: SEM, scanning electron microscope; M O Fe_2O_3-NPs, *Moringa oleifera* Iron oxide nanoparticles.

The anti-migration ability of Fe_2O_3 NPs was studied on MDA-MB 231 cells, following some methods with slight modifications (Kavaz *et al*., 2018). Cells were cultured in 35 mm dishes and lines were drawn on the dishes to create scratch wounds. MDA-MB 231 cells were plated at 1 x 106/mL and 5 x 105/mL per dish; pipette tips were used to create three scratch lines, treated with 50 and 10 µg/mL and incubated for 24 hours. Captured images of the initial and subsequent wounds using a camera attached to an inverted microscope at x100 magnification. Image processing software (ImageJ) was used to analyze the recovery wound area and calculate cell migration using Equation 1.

$$\text{Mo I} = 1 - \left(\frac{Wt}{W0}\right) \quad (1)$$

Mo I, motility index; W_t, the width of the wound at 24 h; $W_{0,}$ initial wound width at 0 h.

STATISTICAL ANALYSIS

We displayed our experiment's results using averages and associated standard deviations. We carefully examined the data using IBM SPSS Statistics version 21 and employed a one-way ANOVA and Student's t-test where applicable. The experiments were conducted three times in triplicate, each time maintaining a sample size of at least n≥3. We considered any P-value below 0.05 as indicative of statistical significance.

RESULTS

The UV-vis validation demonstrated an absorption peak at 314 nm, indicative of the surface plasmon resonance effect associated with the formation of M O Fe_2O_3 NPs, as depicted in fig. 2. The functional groups of M O Fe_2O_3 NPs were determined by analyzing their FTIR spectra within the range of 400 to 4500 cm^{-1}, as depicted in fig. 3. The phase purity of the MO Fe_2O_3 NPs was determined through XRD, as illustrated in fig. 4. The morphology and chemical composition of the synthesized MO Fe_2O_3 NPs were examined using SEM. The results revealed that the MO Fe_2O_3 NPs exhibited an irregular spherical shape without agglomeration, as shown in fig. 5. The EDX spectra utilized to unveil the chemical composition of the MO Fe_2O_3 NPs. The results indicated a predominant presence of Fe and O, along with small amounts of N and Ca, as illustrated in fig. 6. The antimicrobial potential of the M O Fe_2O_3 NPs against *Bacillus cereus* and *Escherichia coli* was shown in table 1.

The impact of varying concentrations (0~500µg/mL) of M O Fe_2O_3 NPs on MDA-MB 231 cells following a 24-hour incubation period was assessed for cytotoxicity and proliferation using the trypan blue assay and MTT assay, respectively (figs. 8a and 9a). In addition, the anti-migratory effect on the cells, was assessed using a wound healing assay (fig. 9b).

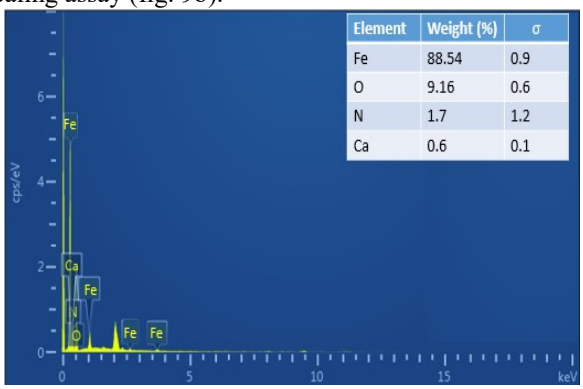

Fig. 6: EDX of the synthesized M O Fe_2O_3-NPs.
Abbreviation: EDX, energy-dispersive X-ray spectroscopy; M O Fe_2O_3-NPs, *Moringa oleifera* Iron oxide nanoparticles.

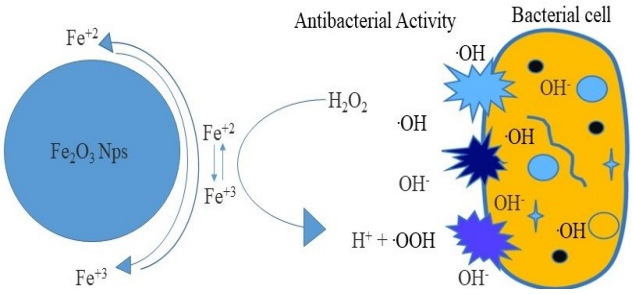

Fig. 7: Predicted antimicrobial potential mechanism of synthesized M O Fe_2O_3-NPs.
Abbreviation: Fe_2O_3-NPs, Iron oxide nanoparticles.

DISCUSSION

Characterization of the synthesized nanoparticles
Fe_2O_3 NPs were synthesized using M. O. leaf extract as a chelating agent (M O Fe_2O_3 NPs). The synthesis process was accelerated owing to the presence of phytoconstituents in the plant extract, which acted as effective reducing agents.

UV-vis spectra analysis was employed to confirm the synthesis of M O Fe_2O_3 NPs nanoparticles shortly after the reaction, evident through a noticeable color change from greenish to reddish-brown. The absorption peak falls within the typical range for Fe_2O_3 nanoparticles, as studies have indicated that Fe_2O_3 nanoparticles exhibit absorption peaks in the range of 295-305 nm (Taffa *et al*., 2015).

The peaks indicated the stretching vibration of Fe-O and Fe-O-H at 764 cm^{-1} and 618 cm^{-1}, respectively, as reported by Mahdavi *et al*. (2013). The involvement of the plant extract in the synthesis of M O Fe_2O_3 NPs was evidenced by the stretching of aliphatic and aromatic N-O amine oxide bands at 841 cm-1 and 1066 cm-1, respectively, as reported by Saravanan *et al*. (2021). Furthermore, prominent peaks at 1971 cm-1 and 2156 cm-1 were associated with the O-H stretching vibration of surface-adsorbed water molecules, as observed in previous studies (Kanagasubbulakshmi and Kadirvelu, 2017). The stabilization and capping of nanoparticles were attributed to the involvement of phytochemicals such as flavonoids and phenols, as revealed by Devatha *et al*. (2016).

The XRD analysis revealed prominent peaks at 012, 104, 110, 113, 202, 024, 116, 018, 214, 300, 208, 1010 and 220, corresponding to 2θ values of 24.05°, 33.01°, 35.53°, 40.74°, 49.31°, 53.87°, 57.41°, 62.27°, 63.85°, 71.69°, 75.32° and 80.51°, respectively. The crystalline nature of the MO Fe_2O_3 NPs was confirmed based on the presence of these peaks, consistent with several studies (Kiwumulo *et al*., 2022). The XRD pattern observed in our synthesized MO Fe_2O_3 NPs suggests the reduction of metal oxide ions by *M. O.* extract and an average crystal size of 19 nm was calculated using Scherrer's equation 1.

Equation (1) describes the calculation of the average crystal size (D) using Scherrer's equation:

In this equation:

$$\text{Crystal size (D)} = \frac{k\lambda}{(\beta \cdot \cos\theta)} \qquad \text{Eq. 1}$$

D represents the average crystal size, k is the shape factor, λ is the wavelength of the X-ray radiation, β is the total width half maximum (FWHM) in radians and θ is the Bragg's angle in radians for Cu-Kα radiation.

The morphology and chemical composition of the synthesized MO Fe_2O_3 NPs were examined using SEM. The results revealed that the M O Fe_2O_3 NPs exhibited an irregular spherical shape without agglomeration, as depicted in fig. 5. This morphology could be attributed to phytochemicals in the M.O. extract. Despite some variability in size, the average size of the nanoparticles, as observed in the SEM image, ranged between 21-26 nm. The surface morphology of the nanoparticles plays a significant role in understanding their behaviour and the contribution of the plant extract to reducing their size has been reported in previous studies (Khadim *et al*., 2022; Abdulaziz *et al*., 2022). In addition, EDX spectra were utilized to unveil the chemical composition of the M O Fe_2O_3 NPs. This outcome provides confirmation of the involvement of the M.O. extract in the synthesis of the nanoparticles. Moreover, elemental mapping analysis demonstrated the distribution of Fe and O within the nanoparticles at 76.23% and 27.40%, respectively.

Antimicrobial activity
The antimicrobial effectiveness of the MO Fe_2O_3 NPs against *Bacillus cereus* and *Escherichia coli* was evaluated and compared to both MO extract and ciprofloxacin (control group). The results demonstrated significant antimicrobial potential against both bacteria, with the synthesized NPs exhibiting pronounced effects on *B. cereus* and *E. coli*. The antimicrobial efficacy of the nanoparticles was notably superior to that of MO methanolic extract ($P<0.0001$; table 1) and ciprofloxacin-treated groups ($P<0.0001$; table 1).

The observed antibacterial potential of the MO Fe_2O_3 NPs against both bacteria may be attributed to the presence of metallic oxide ions in the NPs, while the plant extract showed a comparatively lesser effect. These findings align with previous studies that demonstrated the antimicrobial potential of MO Fe_2O_3 synthesized through biological means against various microorganisms, including *E. coli*, *B. cereus*, *Staphylococcus aureus* and *Pseudomonas aeruginosa* (Huber, 2005; Batool *et al*., 2021; Attia *et al*., 2022). Studies by Rabia *et al*. on Fe_2O_3 NPs synthesized using *Punica granatum* peel extract also support our results (Irshad *et al*., 2017).

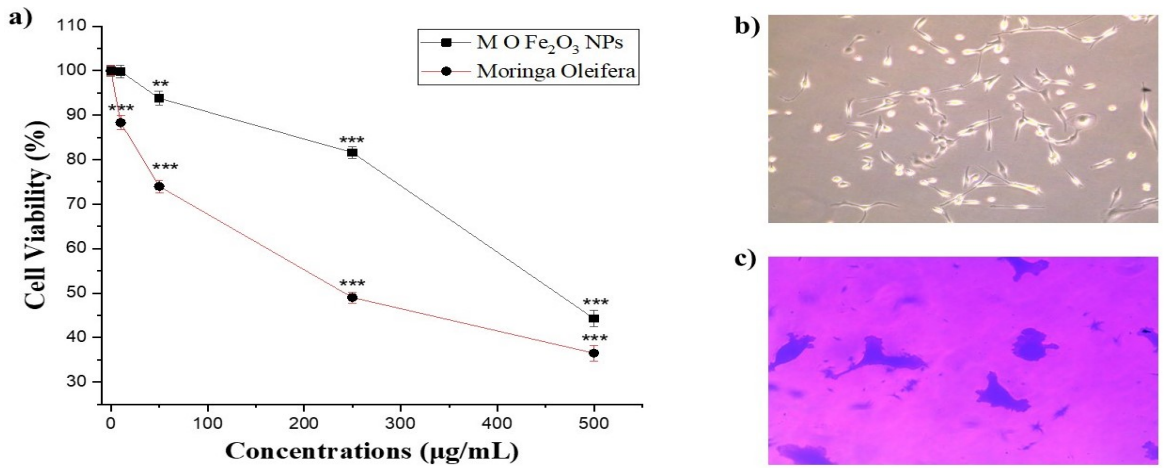

Fig. 8: Effect of various concentrations of synthesized Fe_2O_3-NPs and *Moringa oleifera* on the (a) Viability of MDA-MB 231 cells, (b) Typical phase-contrast light-microscopy image of control (the treated cells), (c) Typical phase-contrast light-microscopy image of the treated cells obtained from tryphan blue exclusion assay.
**P<0.01, ***P<0.0001. Abbreviation: M O Fe_2O_3-NPs, *Moringa Oleifera* Iron oxide nanoparticles.

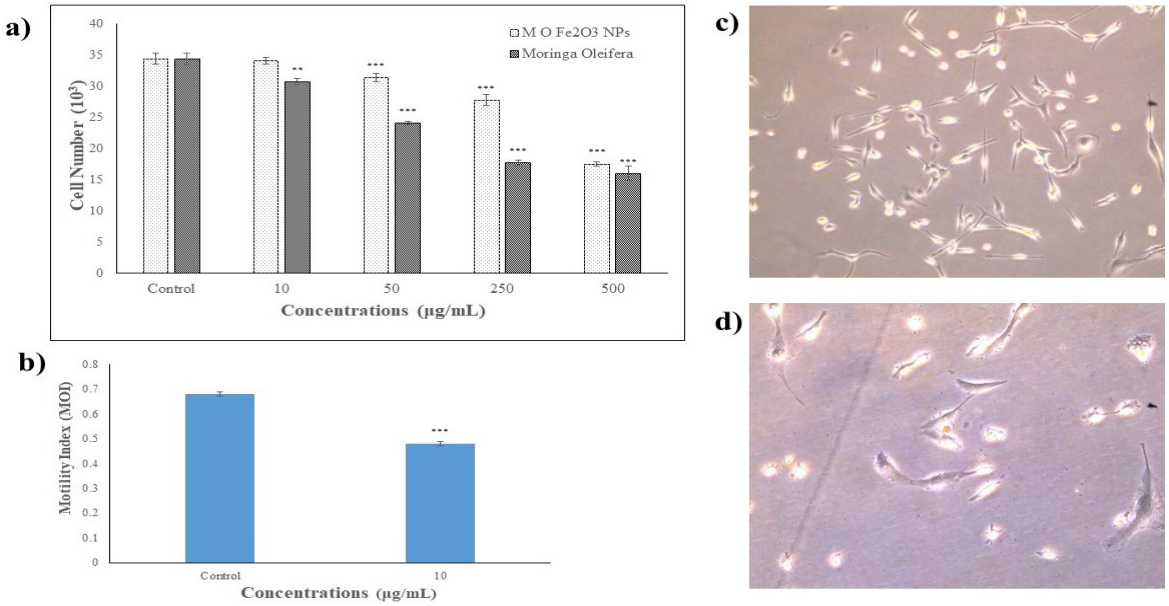

Fig. 9: (a) Effect of various concentrations of synthesized MO Fe_2O_3-NPs and *Moringa oleifera* on the Proliferation of MDA-MB 231 cells, (b) Anti-migratory potential of MO Fe_2O_3-NPs. (c) Typical phase-contrast light-microscopy image of control (the treated cells), (d) Typical phase-contrast light-microscopy image of the treated cells prior to MTT assay. **P<0.01, ***P<0.0001.
Abbreviation: MO Fe_2O_3-NPs, *Moringa oleifera* Iron oxide nanoparticles; MTT, 3-[4,5-dimethylthiazol-2-yl]-2,5-diphenyltetrazolium bromide.

Table 1: (a) Antimicrobial potential of MO Fe_2O_3-NPs and *Moringa oleifera* extract.

Bacterial Strains	*Bacillus cereus* (mean ± SEM)	*Salmonella typhi* (mean ± SEM)	*Escherichia coli* (mean ± SEM)
Standard ciprofloxacin (10 µg/disc)	15.80 ± 0.47	17.54 ± 0.48	15.14 ± 0.31
MO Fe_2O_3 NPs	12.60 ± 0.36***	6.65 ± 0.35***	12.47 ± 0.27***
Moringa oleifera extract	2.50 ± 0.31***	1.97 ± 0.22***	2.49 ± 0.19***

Notes: Results are present as mean ± SEM of inhibition zone (mm) of at least triplicates (n≥3). ***P<0.0001

In our research, the antimicrobial potential is attributed to the release of metallic oxide ions by the NPs (as shown in fig. 7). These ions attach to the bacterial cell wall through electrostatic interaction, targeting thiol functional groups. Subsequently, the Fe_2O_3 NPs can penetrate the cell wall, facilitating nutrient entry. This process ultimately leads to decreased protein levels and cell death, as illustrated in the accompanying predicted mechanism diagram (fig. 7).

Cytotoxic, anti-proliferative* and *anti-migratory potentials

The impact of varying concentrations (0~500µg/mL) of M O Fe_2O_3 NPs on MDA-MB 231 cells following a 24-hour incubation period was assessed for cytotoxicity and proliferation using the trypan blue assay and MTT assay, respectively (figs. 8a and 9a). Light microscopy images of cells treated with different concentrations of MO Fe_2O_3 NPs are also presented in figs. 8b and 9c. The concentrations of MO Fe_2O_3 NPs used in this study were 0, 10, 50, 250 and 500µg/mL and all concentrations demonstrated cytotoxic effects in a concentration-dependent manner. A significant decrease in cell number was observed in cells treated with 50, 250 and 500µg/mL ($P<0.0001$; $n\geq3$). Cells treated with 10µg/mL of the MO Fe_2O_3 NPs did not show any significant changes in cell viability compared to the control group ($P>0.0001$; $n \geq 3$). Similarly, the same concentrations of MO Fe_2O_3 NPs that were toxic to the cells were applied to study their anti-proliferative potential and a significant decrease in cell number was observed in cells treated with 50 250 and 500µg/mL ($P<0.0001$; $n\geq3$). Additionally, 10µg/mL of the synthesized nanoparticles did not show any significant changes in cell viability compared to the control group ($P>0.0001$; $n\geq3$). Similarly, significant decrease in cell number was observed in cells treated with 10 50, 250 and 500µg/mL ($P<0.0001$; $n\geq3$).

These findings are consistent with a study by Susanne *et al*., which reported concentration-dependent cytotoxic and antiproliferative effects on MDA-MB 231 cells treated with Fe_2O_3 NPs. Kossatz *et al*., 2015. Yusefi *et al*. also demonstrated the concentration-dependent cytotoxic potential of Fe_2O_3 NPs against A549, MCF7, HCT116 and HONE1, aligning with our observations on MDA-MB 231 cells (Yusefi *et al*., 2020). The phytochemicals present in the plant extract play a crucial role in the synthesis and stabilization of the nanoparticles, with some exhibiting the ability to inhibit transduction and metastasis in cancer cell lines. The cytotoxic potential observed in our synthesized NPs may be attributed to the release of Fe^{+} from our MO Fe_2O_3 and its involvement in the metabolic activities of the cells (Singh *et al*., 2010). Additionally, the cytotoxic and anti-proliferative effects demonstrated by zinc oxide nanoparticles synthesized using plant extract exhibited a robust impact on the viability of human breast cancer cells, with the effect being concentration-dependent (Prabhakar *et al*., 2017).

MDA-MB 231 cells were subjected to treatment with 500, 250, 50 and 10µg/mL MO Fe_2O_3 NPs and all the concentrations revealed a significant decrease in cell proliferation except 10µg/mL, as shown in 9a and 9b-d. Additionally, the synthesized Fe_2O_3 nanoparticles at concentrations of 10µg/mL that are not toxic and do not affect cell proliferation demonstrated an anti-migratory effect on the cells, as assessed using a wound healing assay (fig. 9b). The motility index of MDA-MB 231 cells markedly decreased with10µg/mL. Furthermore, MO Fe_2O_3 NPs concentrations showed significant differences relative to the control ($P<0.0001$; $n\geq3$; Figure 9b).

These observations align with a study by Li *et al*., which reported that fabricated Fe3O4 nanoparticles capped with polydopamine enhance the migratory potential of mesenchymal stem cells (Li *et al*., 2019). Moreover, medicinal plants containing quercetin as an active ingredient have demonstrated anti-metastatic activity on strongly and weakly metastatic prostate cancer cell models (Li *et al*, 2019; Priya *et al*., 2021; Umar *et al*., 2023).

CONCLUSION

Iron oxide nanoparticles were successfully synthesized through a stable and environmentally friendly green route using *Moringa oleiferea* and characterized through UV-vis, FTIR, XRD, SEM and EDX analyses. The UV-Vis spectra of the synthesized nanoparticles revealed an absorption peak at 314 nm, confirming the successful synthesis and remarkable stability of the nanoparticles. These nanoparticles exhibited a uniform spherical morphology and contained elements such as Fe, O and N, confirming the successful synthesis of MO Fe_2O_3 NPs. Furthermore, the biosynthesized MO Fe_2O_3 NPs demonstrated antimicrobial capabilities against *Escherichia coli* and *Bacillus cereus*. Moreover, the biosynthesized M O Fe_2O_3 NPs exhibited significant anti-migratory potential on MDA-MB 231 human breast cancer cells at lower concentrations of 10µg/mL, while higher concentrations revealed cytotoxic effects on the cells with an IC_{50} of 69.7µg/mL. In summary, stable MO Fe_2O_3 NPs were successfully synthesized using *Moringa Oleiferea* methanolic extract. These synthesized MO Fe_2O_3 NPs and plant extract showed antimicrobial activity against *E. coli* and *B. cereus* and demonstrated cytotoxic, anti-proliferative and anti-migratory effects on highly metastatic human breast cancer cell lines.

REFERENCES

Abdulaziz A, Mohammed S, Alqahtani A M, Mohd A K, Abdullah A, Raisuddin A, Mohsin K, Khalid M and AlGhamdi Rabbani S (2022). Iron oxide nanoparticles: Preparation, characterization and assessment of antimicrobial and anticancer activity. *Adsorp. Sci. Tech.*, **2022**: Article ID 1562051.

Alphandéry E (2020). Iron oxide nanoparticles for therapeutic applications", *Drug Discov. Today*, **25**(1): 141-149.

Amaglo NK, Bennett RN, Lo Curto RB, Rosa EAS, Lo Turco V, Giuffrid A, Lo Curto A, Crea F and Timpo GM (2010). Profiling selected phytochemicals and nutrients in different tissues of the multipurpose tree *Moringa oleifera* L., grown in Ghana. *Food Chem.,* **122**(4): 1047-1054.

Attia N F, El-Monaem E, El-Aqapa H, Elashery S, Eltaweil A, El Kady M, Khalifa S, Hawash H and El-Seedi H (2022). Iron oxide nanoparticles and their pharmaceutical applications. *Appl. Surface Sci. Advan*. **11**: 100284.

Batool F, Iqbal MS, Khan SU, Khan J, Ahmed B and Qadir MI (2021). Biologically synthesized iron nanoparticles (FeNPs) from *Phoenix dactylifera* have anti-bacterial activities. *Sci. Rep.*, **11**: 22132.

Chowdhury P, Roberts AM, Khan S, Hafeez BB, Chauhan SC, Jaggi M and Yallapu MM (2017). Magnetic nanoformulations for prostate cancer. *Drug Discov. Today*. **22**(8): 1233-1241.

Conde-Cid M, Paíga, P, Moreira MM, Albergaria JT, Álvarez-Rodríguez E, Arias-Estévez M and Delerue-Matos C (2021). Sulfadiazine removal using green zero-valent iron nanoparticles: A low-cost and eco-friendly alternative technology for water remediation. *Environ. Res.*, **198:** 110451.

Coppin JP, Xu Y, Chen H Min-Hsiung P, Chi-Tang H, Rodolfo J, James ES, and Qingli W (2013). Determination of flavonoids by LC/MS and anti-inflammatory activity in *Moringa oleifera*. *J. Funct. Foods,* **5**(4): 1892-1899.

Devatha CP, Thalla AK and Katte SY (2016). Green synthesis of iron nanoparticles using different leaf extracts for treatment of domestic waste water. *J. Clean. Prod.*, **139**: 1425-1435.

Dhakad AK, Ikram M, Sharma S, Khan S, Pandey VV and Singh A (2019). Biological, nutritional and therapeutic significance of *Moringa oleifera* Lam. *Phyther. Res.* **33**(11): 2870-2903.

Dowlath MJH, Musthafa SA, Mohamed KSB, Varjani S, Karuppannan SK and Ramanujam G (2021). Comparison of characteristics and biocompatibility of green synthesized iron oxide nanoparticles with chemical synthesized nanoparticles. *Environ. Res.*, **201**(1): bl 111585.

El-Zahaby SA, Elnaggar YSR and Abdallah OY (2019). Reviewing two decades of nanomedicine implementations in targeted treatment and diagnosis of pancreatic cancer: An emphasis on state of art. *J. Control Release*, **10**(293): 21-35.

Fazlzadeh M, Rahmani K, Zarei A, Abdoallahzadeh H, Nasiri F and Khosravi R (2017). A novel green synthesis of zero valent iron nanoparticles (NZVI) using three plant extracts and their efficient application for removal of Cr(VI) from aqueous solutions. *Adv. Powder Technol.*, **28**(1): 122-130.

Gullu H H and Parlak M (2016). Structural characteristics of thermally evaporated Cu 0.5 Ag 0.5 InSe 2 thin films. *Mater. Res. Express*, **3**(5): 055901.

Haocong L, Guan W, Jinpeng L, Kejun N, Jie Z, Lihong G and Yang L (2021). Green synthesis of copper nanoparticles using *Cinnamomum zelanicum* extract and its applications as a highly efficient antioxidant and anti-human lung carcinoma. *J. Exp. Nanosci.*, **16**(1): 410-423.

Huber DL (2005). Synthesis, properties and applications of iron nanoparticles. *Small*. **1**(5): 482-501.

Irshad R, Tahir K, Li B, Ahmad A, Siddiqui R and Azka NS (2017). Antibacterial activity of bhemically capped iron oxide nanoparticles: A view towards green chemistry", *J. Photochem. Photobiol. B, Biol.*, **170**: 241-246.

Kadhim Q, Jabbar Azeez A and Barzinjy Samir MH (2022). Iron oxide nanoparticles: Preparation methods, functions, adsorption and coagulation/flocculation in wastewater treatment. *Environ. Nanotechnol. Monit. Manag.*, **17**(100661): 2215-1532.

Kanagasubbulakshmi S and Kadirvelu K (2017). Green synthesis of Iron oxide nanoparticles using *Lagenaria siceraria* and evaluation of its antimicrobial activity. *Def. Life Sci. J.*, **2**(4): 422-427.

Karima G, Leila R, Kamel M, Abdellah C and Taoufik S (2021). Chemical composition and profile characterization of *Moringa oleifera* seed oil. *S. Afr. Bot.*, **137**(1): 475-482.

Kavaz D, Umar H and Shehu S (2018). Synthesis, characterization, antimicrobial and antimetastatic activity of silver nanoparticles synthesized from *Ficus ingens* leaf. *Artif Cells, Nanomed Biotechnol.*, **46**(Sup3): S1193-S1203.

Kiwumulo HF, Muwonge H, Ibingira C, Lubwama M, Kirabira JB and Ssekitoleko RT (2022). Green synthesis and characterization of iron-oxide nanoparticles using *Moringa oleifera*: A potential protocol for use in low and middle income countries. *BMC Res. Notes*, **15**(1): 149.

Kossatz S, Grandke J, Couleaud P, Latorre A, Aires A, Crosbie-Staunton K, Ludwig R, Dähring H, Ettelt V, Lazaro-Carrillo A, Calero M, Sader M, Courty J, Volkov Y, Prina-Mello A, Villanueva A, Somoza Á, Cortajarena AL, Miranda R, Hilger I (2015). Efficient treatment of breast cancer xenografts with multifunctionalized iron oxide nanoparticles combining magnetic hyperthermia and anti-cancer drug delivery. *Breast Cancer Res.*, **17**(1): 66.

Kumar P, Tomar V, Kumar D, Joshi RK and Nemiwal M (2022). Magnetically active iron oxide nanoparticles for catalysis of organic transformations: A review. *Tetrahedron Lett.*, **106-107:** 132641.

Li X, Wei Z, Lv H, Wu L, Cui Y, Yao H, Li J, Zhang H, Yang B and Jiang J (2019). Iron oxide nanoparticles

promote the migration of mesenchymal stem cells to injury sites. *Int. J. Nanomedicine*, **14**(14): 573-589.

Madubuonu N, Samson O A, Awais A, Ishaq A, Ting-kai Z, Botha S, Maaza M and Fabian IE (2019). Biosynthesis of iron oxide nanoparticles via a composite of *Psidium guavaja-Moringa oleifera* and their antibacterial and photocatalytic study. *J. Photochem. Photobiol. B: Biol.,* **199**: 111601.

Mahdavi M, Namvar F, Ahmad MB and Mohamad R (2013). Green biosynthesis and characterization of magnetic iron oxide (Fe_3O_4) nanoparticles using seaweed (*Sargassum muticum*) aqueous extract. *Molecules*, **18**(5): 5954-5964.

Makkar Harinder PS and Klaus B (1997). "Nutrients and antiquality factors in different morphological parts of the *Moringa oleifera* tree. *J. Agric. Sci.*, **128**: 311-322.

McCright J, Naiknavare R, Yarmovsky J and Maisel K (2022). Targeting lymphatics for nanoparticle drug delivery. *Front. Pharmacol.,* **3**(13): 887402.

Mishra G, Singh P, Verma R, Kumar S, Srivastav S, Jha K and Khosa RL (2011). Traditional uses, phytochemistry and pharmacological properties of *Moringa oleifera* plant: An overview. *Der. Pharm. Lett.,* **3**(2): 141-164.

Morales Morales JA (2017). Synthesis of hematite α-Fe_2O_3 nano powders by the controlled precipitation method/Síntesis de nano polvos de hematita α-Fe_2O_3 por el método de precipitación. *Cienc. en Desarro.*, **8**(1): 99-107.

Prabhakar R, Samadder SR and Jyotsana R (2017). Aquatic and terrestrial weed mediated synthesis of iron nanoparticles for possible application in wastewater remediation. *J. Clean. Prod.*, **168**(1): 1201-1210.

Priya N, Kaur K and Sidhu AK (2021). Green Synthesis: An eco-friendly route for the synthesis of iron oxide nanoparticles. *Front. Nanotechnol.,* **168**(1): 655062.

Promkum C, Kupradinun P, Tuntipopipat S and Butryee C (2010). Nutritive evaluation and effect of *Moringa oleifera* pod on clastogenic potential in the mouse. *APJCP*, **11**(3): 627 - 632.

Saini RK, Manoj P, Shetty NP, Srinivasan K and Girindhar P (2016). Relative bioavailability of folate from the traditional food plant *Moringa oleifera* L. as evaluated in a rat model. *J. Food Sci. Technol.,* **53**(1): 511-520.

Saravanan A, Senthil Kumar P, Varjani Sunita Karishma S, Jeevanantham S and Yaashikaa PR (2021). Effective removal of Cr(VI) ions from synthetic solution using mixed biomasses: Kinetic, equilibrium and thermodynamic study. *JWPE*, **40**(1): 101905.

Singh N, Jenkins G J S, Asadi R and Doak S H (2010). Potential toxicity of superparamagnetic iron oxide nanoparticles (SPION). *Nano Rev.*, **1**(1);PMC3215220.

Suresh J, Pradheesh G, Alexramani V, Sundrarajan M and Hong SI (2018). Green synthesis and characterization of zinc oxide nanoparticle using insulin plant *(Costus pictus D. Don*) and investigation of its antimicrobial as well as anticancer activities. *ANSN*, **9**(1): 015008.

Taffa DH, Hamm I, Dunkel C, Sinev I, Bahnemann D and Wark M (2015). Electrochemical deposition of Fe_2O_3 in the presence of organic additives: A route to enhanced photoactivity. *RSC Advances*. **5**(125): 103512-103522.

Umar H, Kavaz D and Rizaner N (2019). Biosynthesis of zinc oxide nanoparticles using *Albizia lebbeck* stem bark and evaluation of its antimicrobial, antioxidant and cytotoxic activities on human breast cancer cell lines. *Int. J. Nanomedicine*, **14**(1): 87-100.

Umar H, Kavaz D, Abubakar AL, Aliyu MR and Rizaner N (2022). Synthesis of zinc oxide nanoparticles using Ficus thonningii aqueous extract and evaluation of its anti-oxidant and anti-microbial activities. *Bulg. Chem. Commun.*, **54**(3): 277-282.

Umar H, Rizaner N, Usman AG, Aliyu MR, Adun H, Ghali UM, Uzun, OD and Abba SI (2023). Prediction of cell migration in MDA-MB 231 and MCF-7 human breast cancer cells treated with albizia lebbeck methanolic extract using multilinear regression and artificial intelligence-based models. *Pharmaceuticals*, **16**(6): 858.

Waterman C, Cheng DM, Rojas-Silva P, Alexander P, Julia D, Mary A L and Ilya R (2014). Stable, water extractable isothiocyanates from *Moringa oleifera* leaves attenuate inflammation *in vitro*. *Phytochem.,* **103**(1): 114-122.

Xiao-qin L, Daniel W E and Wei-xian Z (2006). Zero-valent iron nanoparticles for abatement of environmental pollutants: Materials and engineering aspects. *Crit. Rev. in Solid State Mater. Sci.*, **31**(4): 111-122.

Yusefi M, Shameli K, Ali RR, Pang SW and Teow SY (2020). Evaluating anticancer activity of plant-mediated synthesized iron oxide nanoparticles using punica granatum fruit peel extract. *J. Mol. Struct.*, **1204**(1): 127539.